Suspension-Induced Stem Cell Transition: A Non-Transgenic Method to Generate Adult Stem Cells from Mouse and Human Somatic Cells

Behzad Yeganeh [1,2]*, Azadeh Yeganeh [3], Kyle Malone [1,4], Shawn T Beug [1,4,5] and Robert P. Jankov [1,2,6]

[1] Molecular Biomedicine Program, Apoptosis Research Centre, Children's Hospital of Eastern Ontario Research Institute; Ottawa, Ontario, CANADA.

[2] Departments of Cellular and Molecular Medicine, Faculty of Medicine, University of Ottawa; Ottawa, Ontario, CANADA.

[3] Molecular Medicine, Peter Gilgan Centre for Research and Learning, SickKids Research Institute; Toronto, Ontario, CANADA.

[4] Departments of Biochemistry Microbiology and Immunology, Faculty of Medicine, University of Ottawa; Ottawa, Ontario; CANADA.

[5] Centre for Infection, Immunity and Inflammation, University of Ottawa; Ottawa, Ontario, CANADA.

[6] Departments of Paediatrics, Faculty of Medicine, University of Ottawa; Ottawa, Ontario, CANADA.

* Correspondence: **author:** Behzad Yeganeh, Ph. D, Apoptosis Research Centre, Children's Hospital of Eastern Ontario Research Institute, 401 Smyth Rd, Ottawa, Ontario CANADA K1H 8L1. Tel: +1 (613) 738-4176; Fax: +1 (613) 738-4847; Email: byeganeh@uottawa.ca or behyeganeh@gmail.com.

Abstract: Adult stem cells (ASCs) can be cultured with difficulty from most tissues, often requiring chemical or transgenic modification to achieve adequate quantities. We show here that mouse primary fibroblasts grown in suspension change from the elongated and flattened morphology observed under standard adherent culture conditions generating rounded cells with large nuclei and scant cytoplasm expressing the mesenchymal stem cell (MSC) marker (Sca1; Ly6A) within 24hrs. Based on this initial observation, we describe here a suspension culture method that, irrespective of the lineage used, mouse fibroblast, primary human somatic cells (fibroblasts, hepatocytes and keratinocytes), is capable of generating a high yield of cells in spheroid form which display expression of ASCs surface markers, circumventing the anoikis which often occurs at this stage. Moreover, mouse fibroblasts-derived spheroids can be differentiated into adipogenic and osteogenic lineages. Analysis of single cell RNA sequence data identified 8 distinct cell clusters with one in particular comprising approximately 10% of the cells showing high levels of proliferative capacity expressing high levels of genes related to MSCs and self-renewal as well as extracellular matrix (ECM). We believe the rapid, high-yield generation of proliferative, multi-potent ASC-like cells by the process we term s̲uspension-i̲nduced s̲tem cell t̲ransition (SIST) could have significant implications for regenerative medicine.

Keywords: Anoikis; Adult stem cells; Somatic cells; Reprograming; suspension-induced stem cell transition; single cell RNA sequence

1. Introduction

Adult stem cells (ASCs) also referred to as somatic or tissue-specific stem cells, are a population of undifferentiated cells that inhabit distinct anatomical locations within specific organs or tissues [1,2]. These cells exhibit the remarkable capacity to differentiate into two or more distinct cell types, each possessing the unique characteristics and functionalities inherent to the tissue- or organ-of-origin [1,2]. This inherent multipotency of ASCs plays a pivotal role in tissue homeostasis, regeneration, and repair, making them indispensable players in the realm of regenerative medicine and biological research. ASCs are commonly isolated and maintained under conventional adherent

culture conditions, where they represent an exceptionally scarce subpopulation of non-adherent cells. These cells possess the unique ability to aggregate and form spherical structures known as "floating spheres," which serve as a hallmark of their stem cell identity. These spheres exhibit distinctive stem cell characteristics, such as self-renewal potential and the capacity to differentiate into multiple cell lineages [3–6]. Recent studies have also shown the use of suspension culture for differentiation of murine and human epidermal stem cells for generation of pluripotent and adult stem cell-derived organoids [7–9].

Our initial observations revealed that when fibroblasts are cultivated in suspension culture, they undergo a notable transformation in morphology and concurrently exhibit the expression of stem cell-associated markers. However, this intriguing phenomenon is transient, as these cells subsequently enter a phase of rapid apoptosis (anoikis or detachment-induced cell death). Therefore, we explored whether ASCs could be derived in larger numbers from suspensions of somatic cells cultured under non-adherent conditions. We initially studied mouse dermal fibroblasts (tail/ear fibroblasts, TEFs) [10] in novel suspension culture conditions together with a newly-formulated growth factor (GF)-enriched [11], serum-free culture media with Rho-kinase inhibitor [12], designed to support the transformation, survival and proliferation of ASCs.

2. Materials and Methods

2.1. Preparation of Tail/Ear Fibroblasts (TEFs)

To establish tail/ear fibroblasts (TEFs), the tails and ears from adult mice (8-12 week-old C57BL/6, FVB, and Ly6a-GFP mice on a B6;129 background) were peeled, minced into 1 cm pieces, placed on culture dishes, and incubated in Dulbecco's Modified Eagle Medium/Nutrient Mixture F-12 (Gibco™ DMEM/F-12, HEPES, Cat#11-330-032, Thermo Fisher Scientific, MA, USA), containing 1% Penicillin and Streptomycin (Cat#15140122, Thermo Fisher Scientific, MA, USA), and 20% heat inactivated fetal bovine serum (FBS; Cat# F1051-500 ml, Sigma-Aldrich, Oakville, ON, CANADA) for 7 days. Cells that migrated out of the graft pieces were transferred to new plates and maintained in DMEM/F-12 supplemented with 10% FBS (passage 2). TEFs from passage 3 were used for all experiments.

2.2. Suspension Culture Methods Causing Cell-Cell Contact

To overcome anoikis, cells were forced into physical contact using one of two methods that achieved similar results.

A) Hanging Drop Suspension Culture in which the force of gravity encourages cell-cell contact. Cells were pretreated for one hour with Rho-kinase inhibitor (ROCKi; Y-27632, 10 μM) and then harvested by trypsinization and seeded at 100 cells per 25 μl drop of DMEM/F-12 supplemented with mouse or human EGF, mbFGF and mIGF-1 (all 20 ng/ml) for TEFs and HDFs, respectively plus 10 μM Y-27632 on the inner side of a 100-mm tissue culture Petri dish lid. For PHHs, Williams Medium E serum-free medium containing hHGF, bFGF and hIGF-1 (all 20 ng/ml) and ROCKi (10 μM) was used and for human keratinocytes, SFM serum-free medium supplemented with hEGF, bFGF and hIGF-1 (all 20 ng/ml) and ROCKi (10 μM). The lid was carefully turned upside down (hanging drop) and placed on top of a Petri dish filled with 5 ml of sterile PBS and the cells cultured in inverted position in separate drops for 2 days. The hanging drops were maintained in a humidified atmosphere 5% CO_2 at 37°C. Cells were monitored under a fluorescence microscope daily to detect creation of aggregates. Images were taken using EVOS FL Auto Cell Imaging System (Thermo Fisher Scientific, MA, USA). On day 3, aggregated cells were transferred to ultra-low attachment (ULA) 96 well plates (Corning® Costar® Ultra-Low Attachment Multiple Well Plate, Cat#7007) containing 200 μl of the same medium in each well. Cells were maintained in 5% CO_2, 21% O_2 and 74% N_2 at 37°C for 7 days. Half of the culture medium was removed and replaced every other day.

B) G-force by Centrifuge (250 × g for 3 min) Cells were plated at 100-300 cells per well in ULA 96 well round-bottom plates (Corning® Costar® Ultra-Low Attachment Multiple Well Plate, Cat#7007) in 200 μl DMEM/F-12 supplemented with mouse or human EGF, mbFGF and mIGF-1 (all 20 ng/ml)

for TEFs and HDFs, respectively plus 10 μM ROCKi on the inner side of a 100-mm tissue culture Petri dish lid. For PHHs, Williams Medium E serum-free medium containing hHGF, bFGF and hIGF-1 (all 20 ng/ml) and ROCKi (10 μM) was used and for human keratinocytes, SFM serum-free medium supplemented with hEGF, bFGF and hIGF-1 (all 20 ng/ml) and ROCKi (10 μM). Cells were maintained in 5% CO_2, 21% O_2 and 74% N_2 at 37ºC for 7 days. Half of the culture medium was removed and replaced every other day.

2.3. Time-Lapse Image Acquisition of Sphere Growth

The growth of spheres was imaged (phase-contrast or and green fluorescence) every 60 minutes using an IncuCyte® live-cell analysis system (Essen BioScience, Ltd, Royston Hertfordshire, UK) equipped with a 20× objective over a 7-day time course.

2.4. Flow Cytometry

A) *For apoptosis assay*, apoptotic cells were quantified using an Annexin V (Alexa Fluor™ 555 conjugate, Cat# A35108, Thermo Fisher Scientific, MA, USA), according to the manufacturer's protocol. Briefly, at the desired time point, both lifted adherent cells or cells in suspension medium were collected by centrifugation at 250 RCF at 4°C for 5 minutes, followed by two cold $1 \times$ PBS washes. Cells were then resuspended in binding buffer (10 mM HEPES, pH 7.4, 140 mM NaCl, 2.5 mM $CaCl_2$) at a concentration of 1×10^6 cells/ml. 100 μl of the cell suspension was transferred to a 5 ml culture tube, and 5 μl of Annexin V (555) was added. Unstained cells were used as negative control. The cells were gently vortexed and incubated in the dark for 15 minutes at room temperature. An additional 200 μl of binding buffer was added to the cell suspension and Cells were analysed *using a BD LSRFortessa™ Cell* Analyzer (BD Biosciences, NJ, USA) to quantify percentages.

B) *Immunophenotype Analysis Using Flow Cytometry:* Antibodies used for immunophenotype analysis of mMSCs and hMSCs surface markers are listed in the supplementary table 1. Cell subsets were stained with antibodies and the isotype control and analysed *using a BD LSRFortessa™ Cell* Analyzer (BD Biosciences, NJ, USA). Collected events per sample numbered 15,000. Data were analyzed using FlowJo software.

2.5. Immunofluorescence (IF) Staining

Immunofluorescence was performed as described previously [13]. Samples (cells and spheroids) were washed with PBS and fixed with 4% paraformaldehyde for 30 min at room temperature. After washing twice with PBS, cells were permeabilized and blocked in a solution of $1 \times$ PBS containing 0.1%–0.5% Triton X-100 and 1% Carbo-Free Blocking Solution (SP-5040-125, Vector Laboratories, Burlingame, CA, USA) for 1h at room temperature. Samples were then incubated with desired primary antibodies at 4°C overnight (list of antibodies and concentrations used can be found in Table 1). After washing three times with PBS, secondary antibodies (1:200, Jackson ImmunoResearch, West Grove, PA, USA) were incubated at 37°C for 1h at room temperature in the dark. Nuclei were stained with DAPI (Roche Life Science) for 15 min. Images were digitally captured using an epifluorescent microscope (Zeiss Axioimager M2 with Apotome 2, Carl Zeiss Microscopy GmbH, Göttingen, Germany) using appropriate filter sets. Identical images acquired with different filter sets were merged using ZEN Pro software (version 2.6, Carl Zeiss Microscopy GmbH).

2.6. Self-Renewal Assay

To assess whether cells within TEF-derived spheroids could be propagated as secondary cultures to determine their self-renewal capacity, we used an established method [3,14] with slight modifications. Spheres were transferred into a small tube and after neutralizing trypsin with media, spheres were mechanically broken down by pipetting the solution up and down with a small pipet tip. Cells were counted using a hemocytometer and trypan blue, single cells were then seeded in 96 well culture plates with 200 μl DMEM/F-12 in each well, supplemented with GFs with a limiting dilution approach and wells containing a single cell were monitored for proliferation and clonal

expansion. The frequency of expansion from single cells was calculated dividing the number of wells containing new spheroids by the total number of wells containing a single cell [3,14].

2.7. In Vitro Differentiation Assays Mouse adipogenic or osteogenic differentiation

Fibroblasts and MSCs-derived spheres were plated in 2-well chamber slide and grown in DMEM/F-12 with 10%. Next day medium was changed to adipogenic or osteogenic differentiation media [15] (StemXVivo steogenic/Adipogenic Base Media, cat# CCM007, RD systems, Minneapolis, MN, USA) and replaced every 3–4 days for a total of 21 days. Adipocyte lipid droplets and osteoblast calcification were detected by oil red O and alizarin red S staining, respectively (Louise Pelletier Histology Core Facility, University of Ottawa)

2.8. Single-cell RNA library preparation and sequencing

SIST cells were prepared according to the protocol described in this study. Between 70,000-100,000 mouse adherence-cultured fibroblasts (monolayer) and dissociated spheroid cells (single cells) were freshly prepared and their gene expression profile analyzed using single-cell 3' RNA-sequencing (StemCore Laboratories, Ottawa General Hospital, U Ottawa). Sequencing libraries were prepared using the Single Cell 3' Reagent Kits V3.1 (10x Genomics, Pleasanton, CA, USA) with the 10X Chromium controller, and sequenced on NextSeq 500 (Illumina, San Diego, CA, USA). Library construction, sequencing, and initial analysis were performed by StemCore Laboratories (Ottawa Hospital Research Institute, University of Ottawa).

2.9. Bioinformatics analysis

Sequencing data were processed with Cellranger v7.0.0 to generate cell vs gene Unique Molecular Identifier (UMI) count matrices using the 10X Genomics mouse genome reference (refdata-gex-mm10-2020-A). Matrices were loaded into R (v4.2.1) and subsequent analysis was performed in Seurat v4.3.0. Data from the attached and suspension culture libraries were separately run through a series of quality control steps, retaining cells with at least 200 detected genes and including only genes detected in more than three cells. The data from each library were processed with scDblFinder v1.10.0 using default parameters to identify potential cell doublets, and each library was filtered to remove doublets and cells with >25% mitochondrial transcripts. UMI counts in the retained cells were normalized using the SCTransform algorithm and the libraries were integrated using the Seurat data integration pipeline with 3000 features. Principal component analysis (PCA) was run on the integrated assay, a nearest neighbour graph was constructed using the first 25 principal components, and cells were clustered using the Louvain algorithm at a resolution of 0.3. Uniform Manifold Approximation and Projection (UMAP) embedding were generated for data visualization, again using the first 25 principal components (integrated UMAP). To visualize differences between the two libraries, SCTransform was run on the raw count data from the combined libraries, followed by PCA and generation of a second UMAP embedding using the first 25 principal components of this new PCA dimensional reduction (SCTransform UMAP). Markers for each cluster were identified using the Seurat FindAllMarkers function with the wilcox test, searching only for markers with a positive log2 fold change. To identify differentially expressed genes between pairs of clusters or between suspension and attached cells the FindMarkers command was used.

2.10. Human Hepatocyte Differentiation

To assess differentiation capacity of PHH-derived spheroids to ductal cells, spheres were seeded in a serum free medium, Williams Medium E containing hHGF, bFGF and hIGF-1 (all 20 ng/ml) until they formed a monolayer. Medium was then changed to Transition and Expansion Medium (TEM) containing DMEM/F12 supplemented with insulin-transferrin-serine (ITS) (Cat# I3146, Sigma-Aldrich, Oakville, ON, CANADA), with the following growth factors or small molecules: hEGF (20 ng/ml, Cat# 78006.1, Stemcell technologies, Vancouver, CANADA), hHGF (20 ng/ml, Cat# 100-39H, Peprotech, Cranbury, NJ, USA), Y27632 (10 μM, Cat# 10005583), CHIR99021 (3 μM, Cat# 13122-1),

Sphingosine-1-phosphate (S1P) (1 μM, Cat#62570), lysophosphatidic acid (LPA) (5 μM, Cat#10010093-1) and A83-01 (1 μM, Cat# 9001799-5) (all from Cayman Chemical, Ann Arbor, Michigan, United States), for 7 days as described previously [16].

2.11. Tumorigenic Assessment of TEF-derived Spheroids

Mouse fibroblast cells and spheres were suspended at $1x\ 10^7$ cells/ml in DMEM/F12 containing 10% FBS. BALB/c Nude mice were anesthetized and 100 μl of the cell suspension (1×10^6 cells) was injected subcutaneously into the dorsal flank. Ninety days after the injection, tissues of the dorsal flank were dissected from the mice, fixed in 4% formaldehyde and embedded in paraffin. Sections underwent hematoxylin and eosin staining and were evaluated by a histopathologist (Dr. A Gutsol).

2.12. Statistics

All numerical data are presented as mean ± SEM from at least three separate experiments. P-values were obtained by 2-tailed *t*-test for 2 groups, or one-way analysis of variance (ANOVA) followed by post hoc Tukey test for more than 2 groups using GraphPad Prism Version 6.0 software (GraphPad Software, San Diego, CA). Differences were considered significant at $P < 0.05$.

3. Results

3.1. Expression of MSC surface markers by mouse TEFs grown in suspension culture while undergoing detachment-induced apoptosis (anoikis)

Stem cell antigen-1 (Sca1; Ly6A) is a well-established marker of murine hematopoietic and mesenchymal stem cells (MSCs) [17]. We used dermal fibroblasts containing a *Ly-6A (Sca-1)* GFP (*Sca-1*-GFP) transgene to monitor conversion of TEFs to MSCs. TEFs from 8- to 12-week-old *Sca-1*-GFP transgene mice [18] were isolated and plated (500 cells/well) on ultra-low attachment (ULA) 96-well plates. Once detached, the elongated and flattened cells transformed to a rounded morphology with large nuclei and scant cytoplasm (**Figure 1A**). Within 24h, an increase in *GFP* expression (endogenous *Sca-1*) was detected (**Figures 1B, C, D and E**). GFP expression was rapidly lost when cells were moved back to adherent culture (**Figure S1A and Movie S1**), suggesting possible conversion of TEFs to MSC-like cells in suspension. Consistent with this interpretation, flow cytometric analysis using mMSCs surface markers [15]: Sca-1, CD29, CD44, CD90.1, CD105, CD106 and CD45R as a negative marker, revealed a transition of wild-type TEFs after 24h suspension culture to a MSC-like phenotype (**Figures 1F**). However, the majority of MSC-like cells derived using this method, which we term Suspension-Induced Stem Cell Transition (SIST), subsequently underwent apoptosis (anoikis) [19], as evidenced by increased expression of Annexin V (**Figures 1G, H**) and cleaved Caspase 3 (**Figure S1B**).

Fig. 1
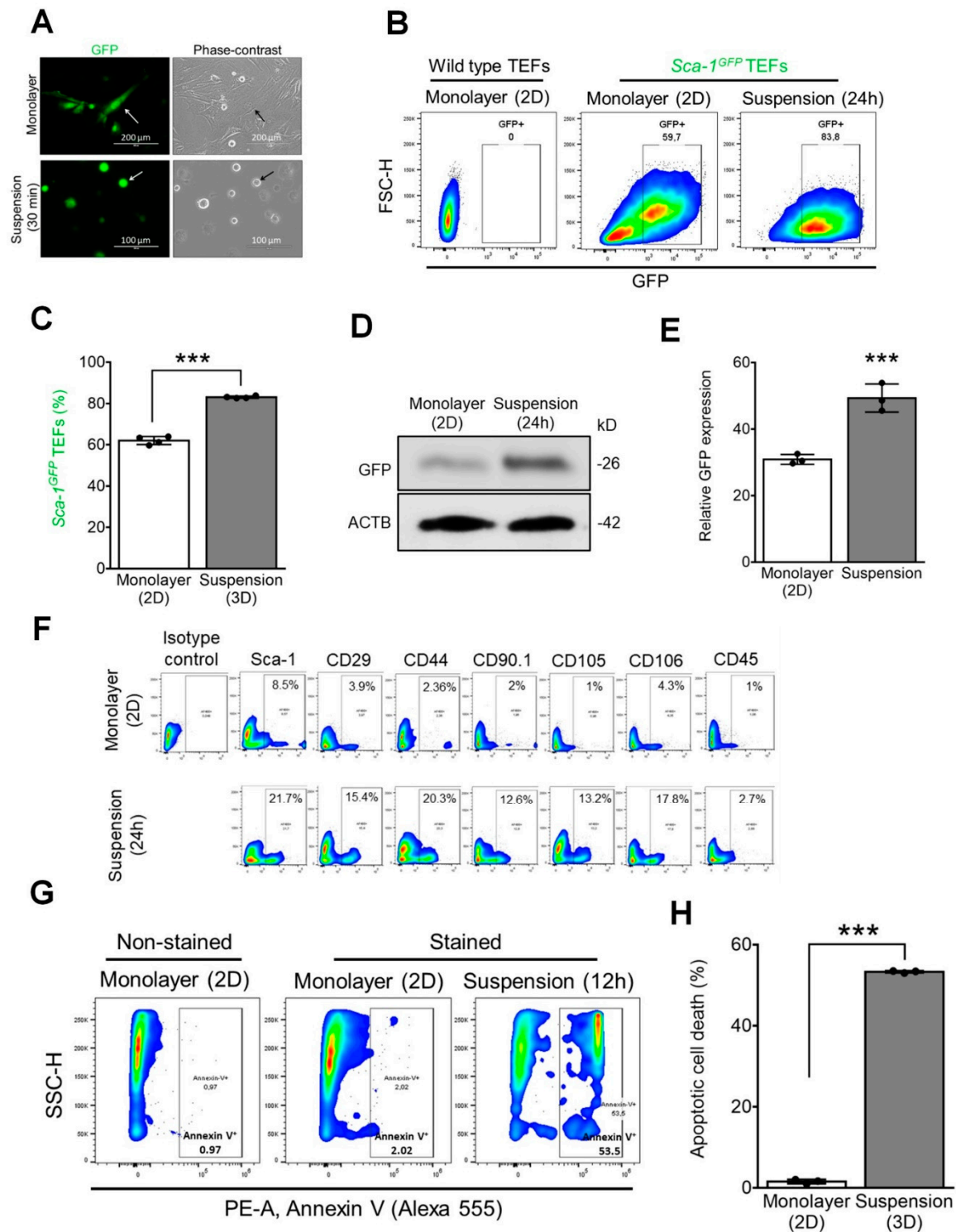
Figure 1. Mouse TEFs grown in suspension culture display MSC surface markers while undergoing detachment-induced apoptosis (anoikis). (A) Comparison of *Sca-1*-GFP TEFs morphology as a monolayer (top) and after 30 minutes in suspension (bottom). GFP fluorescence images are combined with their corresponding phase-contrast images. (B) Flow cytometric analysis of GFP expression of adherent wild-type or *Sca-1*-GFP TEFs cultured as a monolayer and cells cultured in suspension. (C) Quantitative evaluation of GFP expression of adherent *Sca-1*-GFP TEFs from (B). (C) Representative immunoblots of GFP protein in *Sca-1*-GFP TEFs grown as a monolayer and 24 h in suspension. (D) Densitometric analysis of GFP protein expression in monolayer *Sca-1*-GFP TEFs vs suspension (n = 3).

(F) Representative histograms for flow cytometric analysis of wild type mouse TEFs cultured as a monolayer and 24 h in suspension. TEFs were analyzed for mMSCs surface markers, Sca-1, CD29, CD44, CD90.1, CD105, CD106 and CD45R of adherent (top) and suspension cells after 24 h (bottom). (G) Flow cytometry analysis for detection of Annexin V (Alexa 555) of TEFs grown for 14h in adherent or suspension conditions. (H) Quantification of Annexin V positive cells from (F). ***p<0.001.

3.2. Overcoming anoikis with generation of proliferative mouse TEF-derived spheroids expressing MSC markers with self-renewal capacity

It is known that pro-survival signaling pathways are activated by cell-cell and cell-matrix anchorage [20] and that detachment triggers anoikis [21]. We therefore examined whether a modified suspension culture, designed to favor cell-cell contact, may avoid anoikis. TEFs in suspension were brought into physical contact either by gravity, using hanging drop suspension culture (**Figure 2Ai**), or by centrifugation (250 × g for 3 min) in ULA 96-well round-bottom plates (**Figure 2Aii**). The increase of *GFP* expression observed within 24h in spheroids generated by both methods confirmed activation of endogenous *Sca-1,* (**Figure 2B, Movie S2**). For all subsequent experiments, ULA 96-well plates were employed, as they were more suitable for live cell imaging.

Fig. 2
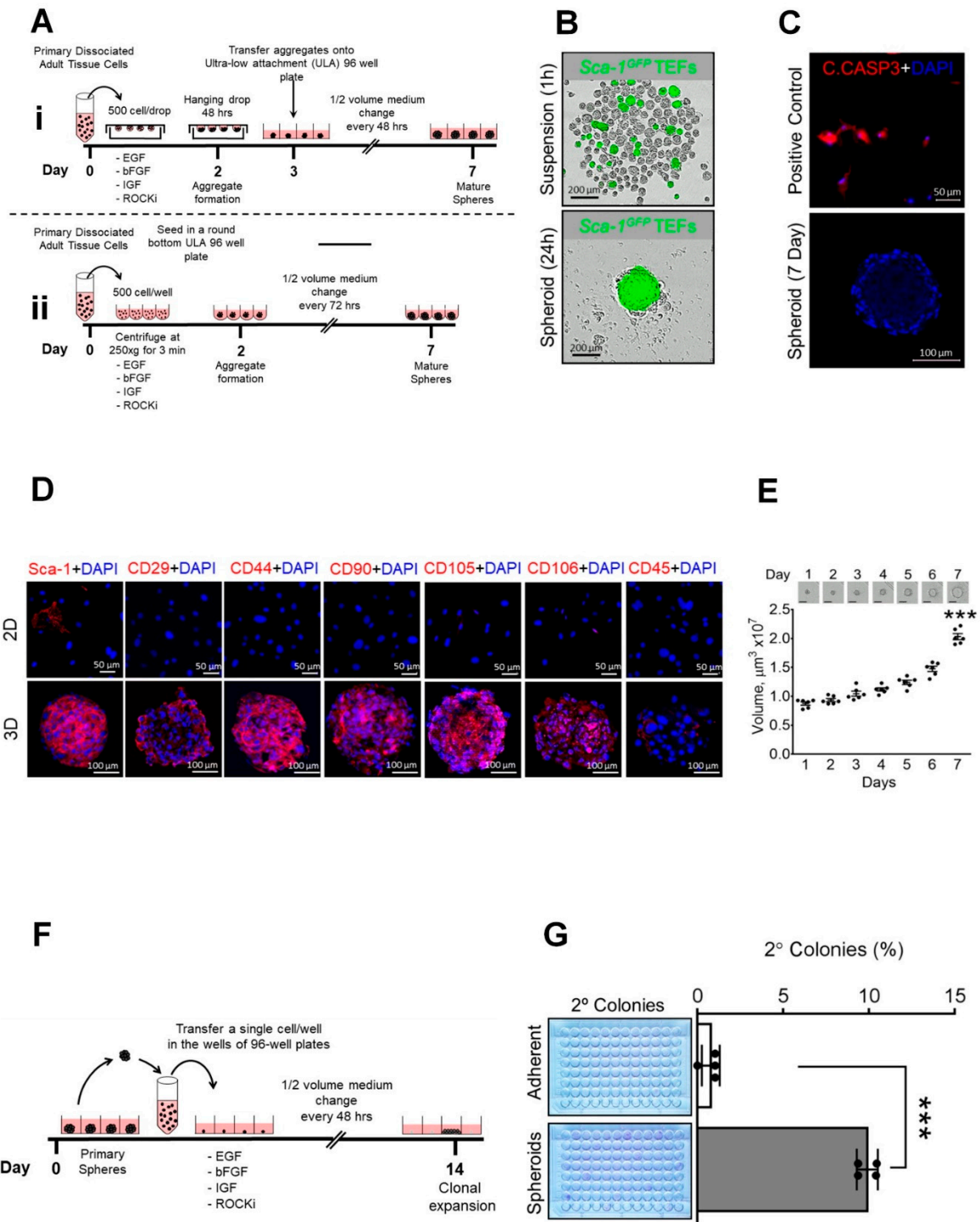
Figure 2. Mouse TEF-derived spheroids grown in SIST express mMSC markers, proliferate and exhibit self-renewal capacity. (A) Schematic representation of two suspension culture methods designed to promote cell-cell contact. **(B)** Representative microscope images captured from live cell imaging from *Sca-1*-GFP fibroblasts grown in suspension culture (left) and sphere formation (right) at 24h. **(C)** IF staining of cleaved caspase 3 (C.CASP3) of mouse TEFs treated with 0.4 mM hydrogen peroxide as positive control (top) and mouse TEFs spheroids after 7 days (bottom). **(D)** IF staining of mouse MSCs-specific surface markers Sca-1, CD29, CD44, CD90.1, CD105, CD106 and CD45R as a negative marker of adherent cells (top) and spheroids (bottom). **(E)** Quantification of spheroid volume over a 7-day time course (n = 6 spheroids). **(F)** Schematic representation of methods used for self-

renewal evaluation of mouse fibroblasts-derived spheroids in this study. **(G)** Representative 96-well plate stained with crystal violet to identify wells with new spheroids. ***p<0.001.

To characterize wildtype TEF-derived spheroids, they were initially transferred to an 8-well chamber slide and allowed to adhere for 1 hour. We first evaluate whether the formation of spheroids using the SIST method reduces anoikis induced by detachment by conducting IF staining using an antibody specific for cleaved caspase 3 (C.CASPASE3). The IF staining for C.CASPASE3 demonstrated the absence of apoptotic cells within the spheroids (**Figure 2C**). We the assessed the expression of mMSC surface markers [15]: Sca-1, CD29, CD44, CD90.1, CD105, CD106 and CD45R as a negative marker via IF. As shown in **Figure 2D**, the majority of cells were positive for MSC markers and negative for CD45R. To evaluate proliferation capacity, spheroid volume was measured over 7 days; a steady growth was observed (**Figure 2E, Movie S3**). To ensure our observations in TEFs were not mouse strain-dependent, spheroid formation was reproduced using TEFs from C57BL/6J and FVB/NJ wild type murine strains (**Figures S1C, D**). To further examine the proliferative capacity of spheroid cells, we stained for the proliferation marker Ki-67 (**Figure S2A**). The proliferative index (proportion of Ki67 positive cells) was significantly increased in spheroids compared to adherent TEFs (**Figure S2B**). Therefore, TEF-derived spheroid cells using our novel SIST platform, remain viable, are highly proliferative and express MSC markers.

We next examined self-renewal capacity of wildtype TEF-derived spheroid cells, using a well-established assay [3]. Spheroids were enzymatically and mechanically dissociated and cells were seeded, one per well, in 96-well plates (288 wells total). The formation of clones was then evaluated after 14 days (**Figure 2F**). As shown in **Figure 2G**, a significant increase in the number of new colonies generated from spheroid cells (9.89%) compared with adherent cells (0.78%) was observed. These observations suggest that SIST spheroids comprise a heterogeneous population of MSCs and progenitor cells without self-renewal capacity. We next examined whether SIST-derived spheroid cells are multipotent. Individual spheres were transferred by micropipette to a 2-well chamber slide. After plating and sphere adherence to the slide, cells were observed to migrate away, causing the gradual loss of three-dimensional structure over a 5-day period (**Figure 3A**). Double IF staining revealed that migrating cells lost their immunoreactivity for Sca-1 and CD44 (**Figure 3B**), similar to loss of *GFP* expression in *Sca-1*-GFP spheroids in adherent culture (**Figure 3A, bottom**). After two days in culture and forming a monolayer, cells were placed either in osteogenic or adipogenic induction culture media for 21 days [15]. Consistent with a degree of differentiation, adipocyte lipid droplets and osteoblast calcification were detected using Oil Red O and Alizarin red S, respectively (**Figure 3C**). To assess for tumorigenic potential, TEFs (control) and spheroid cells were injected into the dorsal flanks of BALB/c nude mice and monitored over three months. No tumors were observed in any mice, which was confirmed by histological examination (**Figure 3D**).

Fig. 3
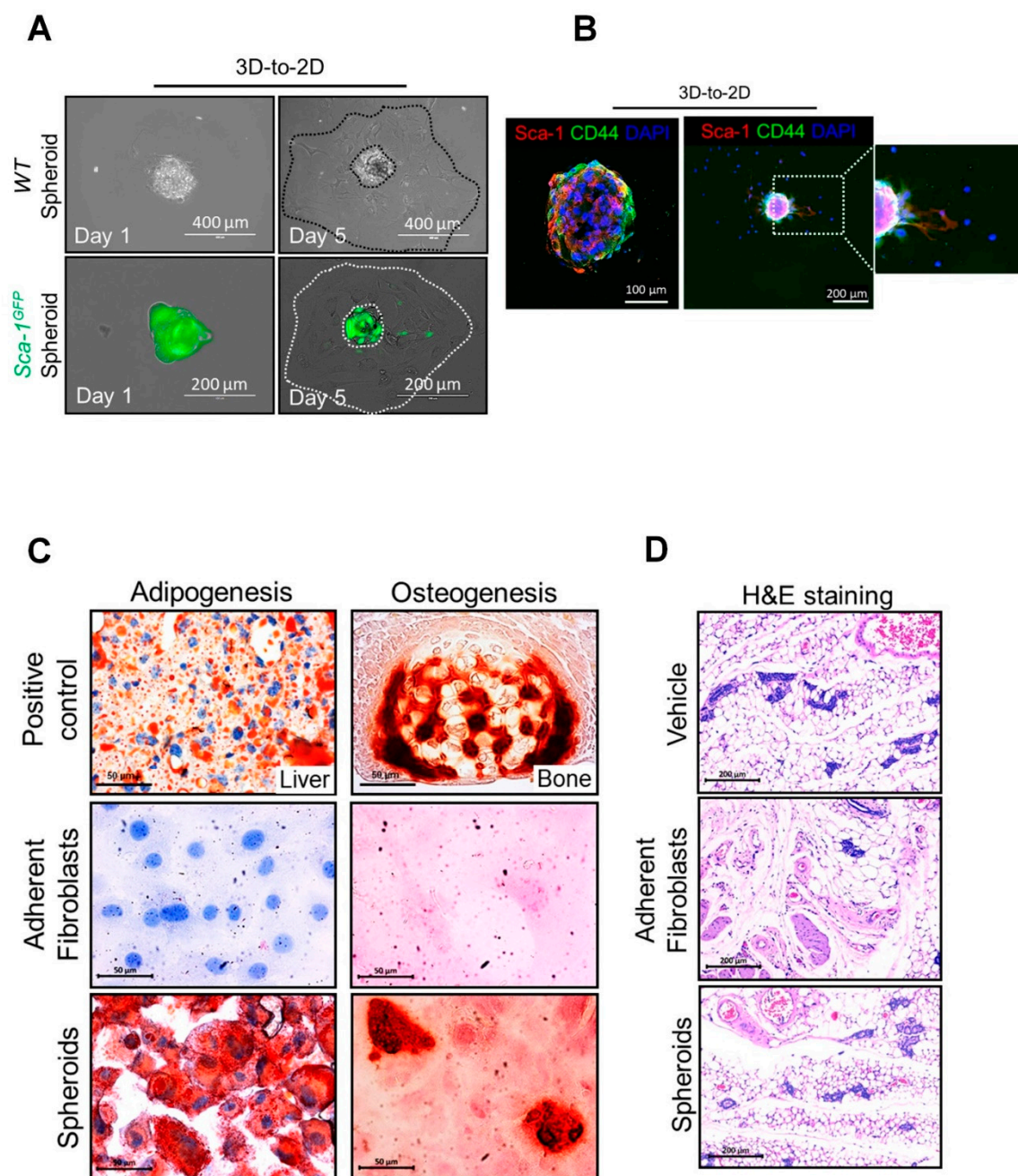
Figure 3. Mouse TEF-derived spheroids are multipotent with no tumorigenic potential. (A) Seeding of a single sphere of wild type (top) and Sca-1-GFP (bottom) fibroblasts on a coverslip after 1 and 5 days in culture. **(B)** Co-IF staining of Sca-1 (red) with another marker of MSCs CD44 (green) in a single sphere after 1 (left panel) and 5 days (right panel) in culture. Scale bars are indicated in the images. **(C)** Representative images for Oil Red O (left) and Alizarin Red S (right) staining demonstrating adipogenic and osteogenic differentiation of adherent fibroblasts (middle panel) compared to TEFs derived from spheroids (bottom panel) compared to adherent fibroblasts (left panel). Mouse liver and bone tissue were used as positive control (top panel). **(D)** Representative hematoxylin and eosin staining of tissues dissected from injection sites in mice receiving cell-free vehicle (Vehicle), adherent monolayer fibroblasts or spheroid-derived cells (Spheroids).

3.3. Characterizing the global gene expression profile of mouse TEF-derived spheroids compared to monolayer culture

To identify the transcriptional changes resulting from growth in spheroid vs. monolayer conditions we performed single cell RNA sequencing (scRNA-seq) on cells grown under both conditions. After quality control steps to remove presumed low viability cells (>25% mitochondrial transcripts) and cell doublets, a total of 11,515 cells (8,022 from spheroid culture, and 3,493 from monolayer culture) were retained for analysis. Data from the two libraries were combined using the Seurat integration pipeline to group similar cells from both libraries and the data were visualized using Uniform Manifold Approximation and Projection (UMAP). A nearest neighbor graph was constructed using the integrated assay and clustering was performed using the Louvain algorithm at a resolution of 0.3, identifying eight clusters (**Figure 4A**). Coloring cells by source library in the UMAP projection shows that the integration procedure intermixed cells from the two libraries in UMAP space, compared to a UMAP projection generated on the non-integrated data, in which the cells from the two libraries are separate in UMAP space (**Figure S3A**). The cells of both libraries can also be split into populations with a high (>2,500) or low (≤2,500) number of detected genes, with an increased number of lower gene count cells from the spheroid culture (**Figure S3B**).The low and high gene cells group separately in UMAP space and Louvain clustering, with clusters 0, 1, 2, and 6 containing the low gene cells, and clusters 3, 4, 5, and 7 containing high gene cells. Identification of marker genes for each cluster found between 233 and 1,671 markers per cluster (with an adjusted p-value <0.05), with a total of 3,365 genes identified as markers of at least one cluster. In these clusters, spheroid cells comprise the majority of clusters 0, 1, 2, 4 and 7 (**Figure S3C**). The heatmap suggested differential gene expression across all clusters (**Figure S3D**), which supports their separate distribution in UMAP (**Figure 4B**). As seen in **Figure S3D**, clusters 1 and 6 grouping together in the top dendrogram, as do clusters 4 and 7; these cluster pairs were both grouped as a single cluster when the clustering was run at a lower resolution. Analysis of differentially expressed genes (DEGs) revealed that each cluster was characterized by a specific transcriptional profile (Supplementary Excel spreadsheet 1).
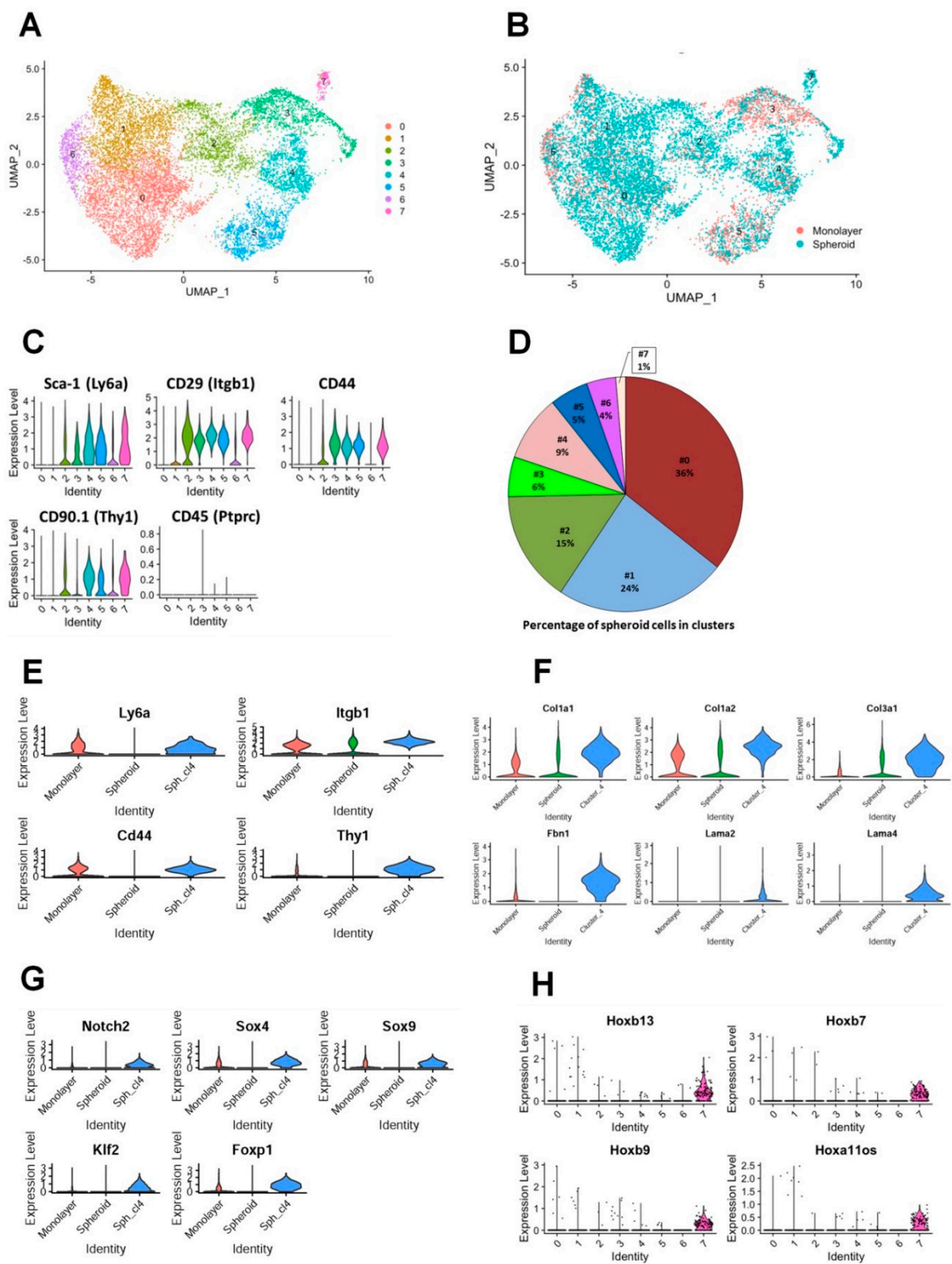
Figure 4. Characterization of mouse TEF-derived spheroids vs. monolayer by differential expression gene analysis. (A) UMAP projection of cells calculated from a Principal Component Analysis (PCA) reduction of the Seurat integrated assay, which attempts to bring similar cells close together. Cells are colored by **(A)** cluster, identified from the integrated assay at a resolution of 0.3 or by **(B)** source library showing the overlap of UMAP coordinates. **(C)** Violin plots of MSC surface markers genes observed in IF staining in Figure 2C, showing expression profiles split by source library within each cluster. **(D)** Pie chart demonstrating distribution of the spheroid cells across clusters. **(E)** Violin plot visualization of expression of MSC surface markers genes identified as significantly enriched in cluster 4. **(F)** Violin plot visualization of expression of selected collagen, fibronectin and laminin genes identified as significantly enriched in cluster 4. **(G)** Violin plots of stem cell self-renewal

genes identified as significantly enriched in cluster 4. **(H)** Violin plot visualization of expression of homeobox genes identified as significantly enriched in cluster 7.

Next we examined expression of the MSC surface markers observed in IF staining (**Figure 2C**) in each cluster. Consistent with the IF results in **Figure 2C**, the expression levels of mouse MSC genes, *Sca-1* (*Ly6a*), *CD29* (*Itgb1*), *CD44*, *CD90.1* (*Thy1*) were high in clusters 2, 3, 4, 5 and 7 (**Figures 4C and S4**). On the basis of their gene expression profile, we focused on clusters 4 and 7 for further analysis. Our gene expression analyses revealed that cluster 4, which includes 9% of 8,022 original spheroid cells (**Figure 4D**), exhibited significantly increased expression of MSC markers compared to the rest of the cells (**Supplementary Excel spreadsheet 2, and Figure 4E**). We observed that the expression of many extracellular matrix (ECM) genes, including *Col1a1, Col1a2, Col3a1, Fbn1, Lama2, and Lama4*, were significantly greater in cells of one of more of clusters 2, 3, 4, 5 and 7 (**Table S1 and Figures S5A, B**), and that expression of some of these genes was significantly higher in spheroid than in attached cells. Further, their expression was significantly increased in spheroid cells of cluster 4 compared with the rest of the cells (**Figure 4F**). Since approximately 10% of spheroids cells showed self-renewal property (**Figure 2F**), we sought to explore the genes important for stem cell self-renewal. Analysis of differentially expressed genes revealed significantly increased expression of one or more of the genes *Notch2, Sox4, Sox9, Klf2*, and *Foxp1* [22–26] in clusters 3, 4, 5 and 7 (**Table S2 and Figure S6A**), but only in cluster 4 was expression all of these genes significantly greater when compared to the remainder of the dataset, with *Sox9* and *Foxp1* also significantly higher in spheroid vs monolayer cells within cluster 4 (**Table S2 and Figures 4G and S6B**). The heatmap shown in **Figure S6C** displays expression profile of selected self-renewal and collagen genes across clusters. The DEGs analysis of cluster 7, which had the lowest percentage of spheroid cells among the clusters (**Figure 4D**), showed significant upregulation of a family of transcription factors, *Hox* genes [27], including *Hoxb7, Hoxb9, Hoxb13,* and *Hoxa11os* (**Figures 4H and S7A**) and *Mmp10* and *Mmp13* genes which are implicated in ECM remodeling [28] (**Figures S7B, C**). The heatmaps demonstrating average normalized expression per cluster of genes expressed at a significantly higher level in cluster 7 and all the *Hox* and *Mmp* genes in the dataset is presented in Figures S8A, B. Altogether, characterization of transcriptional profiles of the TEFs-derived spheroid cells using scRNA sequencing revealed the presence of specific clusters associated with mesenchymal stem-like cells and self-renewing capacity.

3.4. Generation of spheroids with SC properties from cells of all three human germ layers, mesoderm, endoderm and ectoderm (human dermal fibroblasts, hepatocytes and keratinocytes, respectively.

We next assayed SIST on primary human dermal fibroblasts (HDFs), which revealed a transition of HDFs after 24h suspension culture to a MSC-like phenotype as evident by flow cytometric analysis using hMSCs surface markers [15]: CD105, CD106, CD146, CD166, STRO-1 and CD45 (negative marker) (**Figure 5A**). HDFs also showed a capacity to form a growing spheroid similar to mouse TEFs (**Figures 5B, S9A and Movie S4**). Stem cell characteristics were confirmed by IF staining using human MSC-specific surface markers [15] CD105, CD106, CD146, CD166, STRO-1 and CD19 and CD45 (negative marker), (**Figure 5C**). Also similar to TEFs, MSC markers were lost when spheroids were transformed to an adherent monolayer (**Figures S9B, C**).

Fig. 5
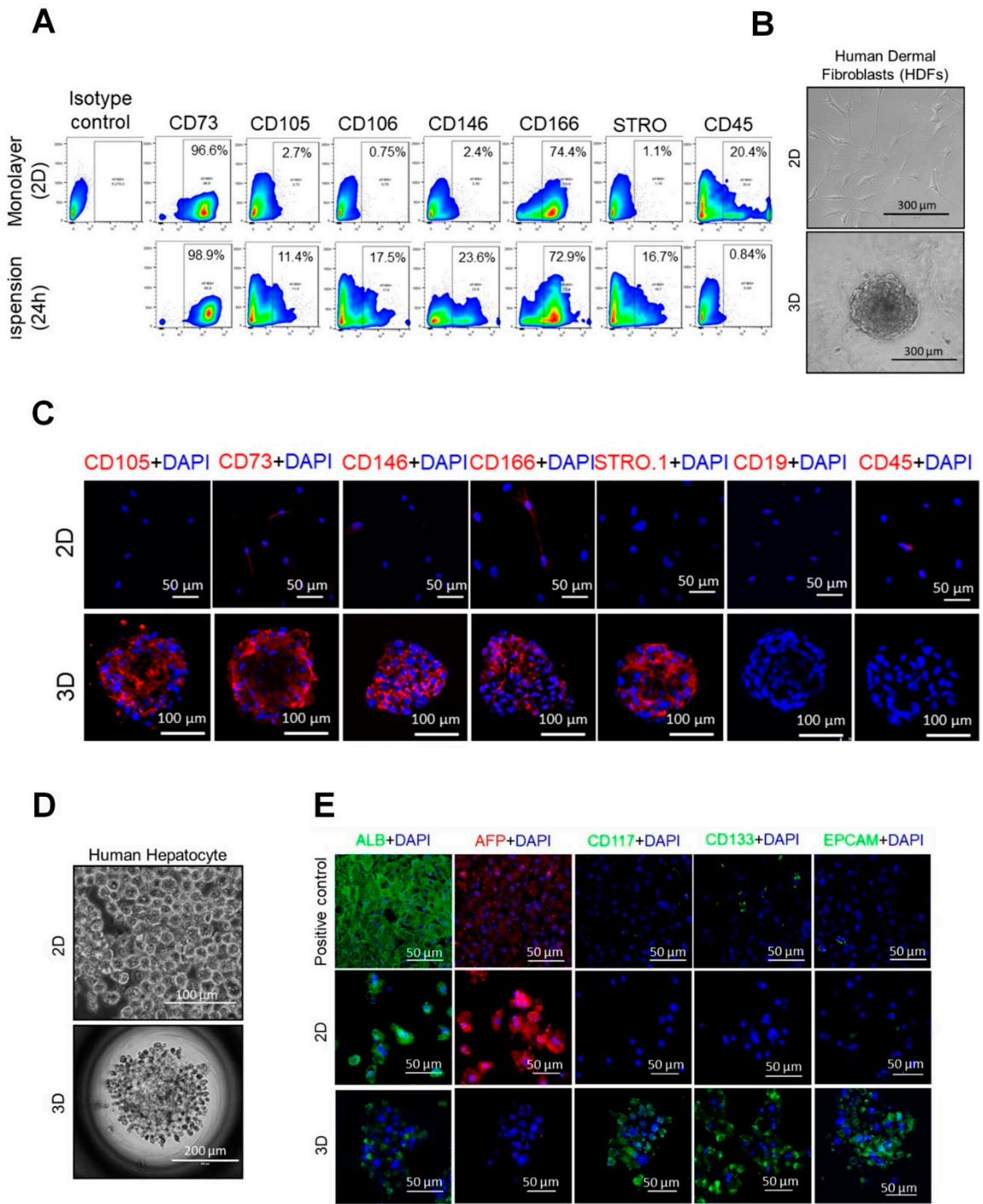
Figure 5. Human dermal fibroblast- and hepatocyte-derived spheroids possess SC properties. (A) Representative phase contrast images of adherent monolayer human dermal fibroblasts (top) and a spheroid after 7 days in culture (bottom). **(B)** Representative histograms for flow cytometric analysis of primary HDFs cultured as a monolayer and 24 h in suspension. HDFs were analyzed for surface hMSCs surface markers, CD73, CD105, CD106, CD146, CD166, STRO-1 and CD45 as a negative marker of adherent (top) and suspension cells after 24 h (bottom). **(C)** IF staining of human MSC-specific surface markers CD73, CD105, CD106, CD146, CD166, STRO-1 and CD45 as a negative marker of adherent cells (top) and spheroids (bottom). **(D)** Representative phase contrast images of adherent monolayer human hepatocytes (top) and a spheroid after 7 days in culture (bottom). **(E)**

Characterization of human hepatocyte-derived spheroids by IF staining using human hepatic stem cell-specific surface markers CD117, CD133, EPCAM, and AFP and ALB as a hepatocyte marker on adherent cells (top) and spheroids (bottom). Sections from human liver tissue were used as positive control (top panel). Scale bars are indicated in the images.

Finally, we examined whether other human somatic cells of endodermal (hepatocyte) or ectodermal (keratinocyte) origin could also undergo SIST. Primary human hepatocytes (PHHs) formed spheres (**Figure 5E**) that were less compact than TEF and HDF-derived MSCs spheroids, but which nevertheless expressed human hepatic stem cell-specific surface markers CD117, CD133, EPCAM and were negative for the hepatocyte marker, AFP [16] (**Figure 5F**). As for mesodermal cells, stem cell markers were lost when PHH-derived spheroids formed an adherent monolayer (**Figures 6A, B**). To confirm that PHH-derived spheroid cells are capable of differentiation to ductal cells, spheroids were grown to form a monolayer using an established transition and expansion medium for 7 days [16] and then showed to stain for CK19 (**Figure 6C**), a specific ductal cell marker [16,29]. Primary human keratinocytes also generated proliferating spheres (**Figure 6D**) which were positive for stem cell markers, TfR/CD71 and p63/TP73L [30–32], and negative for keratinocyte markers, CK1 and CK5 and CK14 [32,33] (**Figure 6E**). Collectively, our results confirm transformation of mouse and primary human somatic cells (originated from all three germ layers) to ASC-like cells when subjected to unique SIST suspension culture conditions designed to avoid anoikis.

Fig. 6
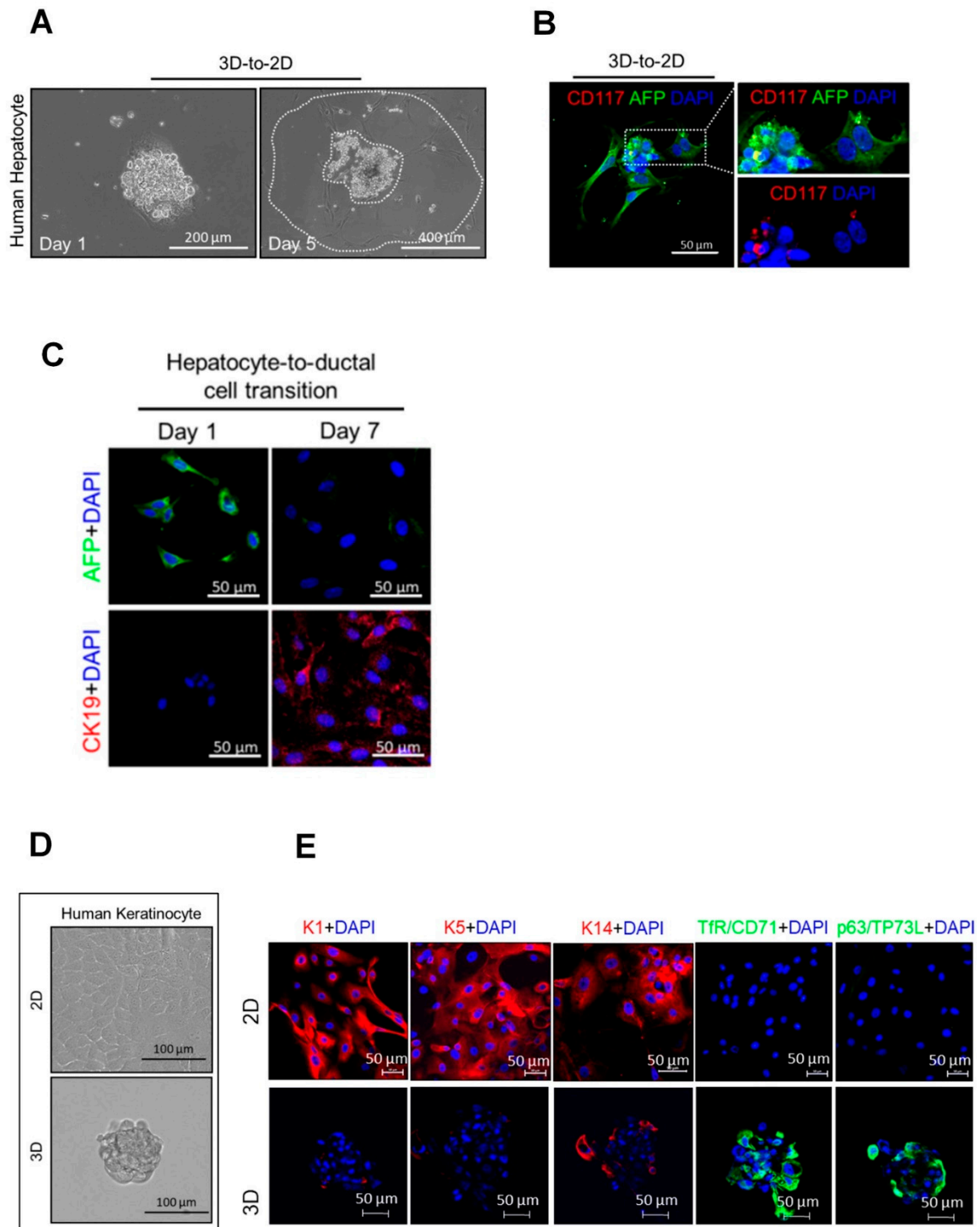
Figure 6. Differential capacity of human hepatocyte-derived spheroids and formation of spheroids by human keratinocytes that proliferate and express keratinocyte-specific stem cell markers. (A) A single sphere of human hepatocytes after seeding on coverslip at day 1 (left) and day 5 (right) in culture. (B) Co-IF staining of CD117 (red) with AFP (green) in a single sphere after 3 days in culture. (C) IF staining of AFP (green) and CK19 (red, ductal cell marker) on human hepatocytes derived from spheroids after 7-days culture in transition/expansion medium. (D) Representative phase contrast images of monolayer human keratinocytes (top) and a spheroid at day 7 (bottom). (E) IF staining of human keratinocytes CK1, CK5 and CK14 and keratinocyte stem cell markers TfR/CD71 and p63/TP73L on adherent cells and spheroids. Scale bars are indicated in the images.

4. Discussion

Herein, we report a novel suspension culture method that circumvents anoikis, thus allowing a comparatively large proportion of mouse and human somatic cells to form spheroids enriched with cells that have ASC-like properties. We believe the conditions that favor growth of ASCs in a non-adherent culture environment resulted from increased cell-cell contact in conjunction with optimized culture media. The mechanisms by which normal cells in non-adherent culture acquire ASC characteristics remain unclear. Most primary cells are considered to be anchorage dependent for survival with anoikis rapidly ensuing once they are detached, complicating examination of their properties in non-adherent culture [19,21]. In contrast, adherence to plastic substrate leads to the induction of a transcriptional and surface marker shift allowing for survival [34]. Unlike normal cells, transformed or tumorigenic epithelial cells can proliferate when non-adherent, allowing an epithelial-mesenchymal transition (EMT) with emergence of cells with stem cell properties [35]. In contrast, the suspension culture method herein termed SIST, encourages physical contact of cells to allow normal cells to avoid anoikis, thereby more efficiently forming spheroids containing ASC-like cells.

One of the first morphological changes we observed in cells grown in suspension culture was their transformation into clusters of round-shaped cells with large nuclei and scant cytoplasm, possibly reflecting a mesenchymal to epithelial transition (MET). Recent studies have shown that generation of induced pluripotent stem cells from mouse fibroblasts requires the activation of intracellular MET signals [36,37] suggesting a cooperative process between exogenous transcription factors and the extracellular micro-environment. In accord, our scRNA-seq analysis revealed cellular and transcriptional modules associated with ECM, MScs and stem cell self-renewal. Therefore, our observations raise the possibility that somatic cells are intrinsically capable of transforming into ASCs in non-adherent culture conditions by activating signaling pathways similar to that observed in MET.

Importantly, ASC-like cells generated using SIST appear to have normal morphology while lacking tumorigenicity. Furthermore, using this strategy, the derivation of ASCs from the same tissue can effectively uphold their intrinsic cellular phenotype while substantially mitigating the risk of perturbations in their epigenetic memory. Thus, this method stands as a promising avenue for obtaining stem cells that closely mirror their tissue of origin, thereby ensuring the preservation of their characteristic epigenetic signatures. This is advantageous, given that induced cells inherit numerous components of epigenetic memory from donor tissues, which represents a potential safety concern in the clinic [38]. Such precision in epigenetic maintenance holds particular significance in the realm of regenerative medicine, as it fosters the development of cells that exhibit a heightened resemblance to their in vivo counterparts, enhancing their suitability for therapeutic applications and tissue regeneration.

Although the results of SIST obtained from cells of mesodermal origin were reproduced in human endoderm and ectoderm cells, spheres formed by human hepatocytes and keratinocytes were less dense and smaller than those derived from mouse and human fibroblasts. This could be due to differences in the basic growth requirements of somatic cells from diverse germ layer origins and could potentially be overcome by further modification of the culture media. Certainly, more work is required to improve the efficiency of ASC-enriched sphere formation from somatic cells derived from diverse tissues. Nevertheless, our results suggest that normal somatic cells can represent a rapid and high-yield source of ASCs, which could have important implications for regenerative medicine.

Supplementary Materials: The following supporting information can be downloaded at the website of this paper posted on Preprints.org.

Funding: This work was supported by operating funding from the Canadian Institutes of Health Research (FRN162226 to RPJ) and by J.P. Bickell Foundation Medical Research Grant and CHEO Research Institute Research Growth Award (to BY).

Institutional Review Board Statement: All mice were maintained and handled in strict accordance with good animal practice and animal studies were conducted according to criteria established by the Canadian Council on Animal Care and were approved by the University of Ottawa Animal Care Committee.

Data Availability: Data are contained within the article. Feature-barcode matrices and raw sequence data have been deposited in the Gene Expression Omnibus (GEO, https://www.ncbi.nlm.nih.gov/geo/query/acc.cgi?acc=GSE241814) and are available under the accession number [czwxugschfgplub]."

Acknowledgments: We thank J Berman, A MacKenzie, WL Stanford, and B Thébaud for helpful scientific discussions and for their critical reading of the manuscript. The authors would like to acknowledge the assistance of StemCore Laboratories Genomics Core Facility (OHRI, uOttawa), RRID: SCR_012601 and the assistance of the Ottawa Bioinformatics Core Facility (uOttawa/OHRI), RRID:SCR_022466. We also thank A Gutsol (University of Ottawa) for histopathological evaluation of the BALB/c Nude mice, N Earl and W Mears for technical assistance and MJ Chen and MZ Lai (Institute of Molecular Biology, Academia Sinica, Taipei, Taiwan) for generous provision of the *Sca-1*-GFP TEFs.

Conflicts of Interest: The authors declare no conflict of interest.

References:

1. Slack, J.M., *Origin of stem cells in organogenesis.* Science, 2008. 322(5907): p. 1498-501.
2. Clevers, H., *STEM CELLS. What is an adult stem cell?* Science, 2015. 350(6266): p. 1319-20.
3. Reynolds, B.A. and S. Weiss, *Generation of neurons and astrocytes from isolated cells of the adult mammalian central nervous system.* Science, 1992. 255(5052): p. 1707-10.
4. Toma, J.G., et al., *Isolation of multipotent adult stem cells from the dermis of mammalian skin.* Nat Cell Biol, 2001. 3(9): p. 778-84.
5. Dontu, G., et al., In vitro *propagation and transcriptional profiling of human mammary stem/progenitor cells.* Genes Dev, 2003. 17(10): p. 1253-70.
6. Beltrami, A.P., et al., *Adult cardiac stem cells are multipotent and support myocardial regeneration.* Cell, 2003. 114(6): p. 763-76.
7. Takahashi, J., et al., *Suspension culture in a rotating bioreactor for efficient generation of human intestinal organoids.* Cell Rep Methods, 2022. 2(11): p. 100337.
8. Capeling, M.M., et al., *Suspension culture promotes serosal mesothelial development in human intestinal organoids.* Cell Rep, 2022. 38(7): p. 110379.
9. Boonekamp, K.E., et al., *Long-term expansion and differentiation of adult murine epidermal stem cells in 3D organoid cultures.* Proc Natl Acad Sci U S A, 2019. 116(29): p. 14630-14638.
10. Takahashi, K. and S. Yamanaka, *Induction of pluripotent stem cells from mouse embryonic and adult fibroblast cultures by defined factors.* Cell, 2006. 126(4): p. 663-76.
11. Bafico, A. and S.A. Aaronson, *Classification of Growth Factors and Their Receptors.* 6th ed. Holland-Frei Cancer Medicine, ed. D.W. Kufe, et al. 2003, Hamilton (ON): BC Decker Inc.
12. Watanabe, K., et al., *A ROCK inhibitor permits survival of dissociated human embryonic stem cells.* Nat Biotechnol, 2007. 25(6): p. 681-6.
13. Yeganeh, B., et al., *Autophagy is required for lung development and morphogenesis.* J Clin Invest, 2019. 129(7): p. 2904-2919.
14. Weiss, S., et al., *Multipotent CNS stem cells are present in the adult mammalian spinal cord and ventricular neuroaxis.* J Neurosci, 1996. 16(23): p. 7599-609.
15. Keating, A., *Mesenchymal stromal cells: new directions.* Cell Stem Cell, 2012. 10(6): p. 709-716.
16. Wu, H., et al., *Reversible transition between hepatocytes and liver progenitors for* in vitro *hepatocyte expansion.* Cell Res, 2017. 27(5): p. 709-712.
17. Bonyadi, M., et al., *Mesenchymal progenitor self-renewal deficiency leads to age-dependent osteoporosis in Sca-1/Ly-6A null mice.* Proc Natl Acad Sci U S A, 2003. 100(10): p. 5840-5.
18. Miles, C., et al., *Expression of the Ly-6E.1 (Sca-1) transgene in adult hematopoietic stem cells and the developing mouse embryo.* Development, 1997. 124(2): p. 537-47.
19. McGill, G., et al., *Loss of matrix adhesion triggers rapid transformation-selective apoptosis in fibroblasts.* J Cell Biol, 1997. 138(4): p. 901-11.
20. Frisch, S.M. and R.A. Screaton, *Anoikis mechanisms.* Curr Opin Cell Biol, 2001. 13(5): p. 555-62.
21. Frisch, S.M. and H. Francis, *Disruption of epithelial cell-matrix interactions induces apoptosis.* J Cell Biol, 1994. 124(4): p. 619-26.
22. Yartseva, V., et al., *Heterogeneity of Satellite Cells Implicates DELTA1/NOTCH2 Signaling in Self-Renewal.* Cell Rep, 2020. 30(5): p. 1491-1503 e6.
23. Larsimont, J.C., et al., *Sox9 Controls Self-Renewal of Oncogene Targeted Cells and Links Tumor Initiation and Invasion.* Cell Stem Cell, 2015. 17(1): p. 60-73.
24. Wang, H., et al., *Klf2 contributes to the stemness and self-renewal of human bone marrow stromal cells.* Cytotechnology, 2016. 68(4): p. 839-48.
25. Pearson, C.A., et al., *Foxp1 Regulates Neural Stem Cell Self-Renewal and Bias Toward Deep Layer Cortical Fates.* Cell Rep, 2020. 30(6): p. 1964-1981 e3.

26. Zhang, L., et al., *Sox4 enhances chondrogenic differentiation and proliferation of human synovium-derived stem cell* via *activation of long noncoding RNA DANCR.* J Mol Histol, 2015. 46(6): p. 467-73.

27. Leclerc, K., et al., *Hox genes are crucial regulators of periosteal stem cell identity.* Development, 2023. 150(6).

28. Stamenkovic, I., *Extracellular matrix remodelling: the role of matrix metalloproteinases.* J Pathol, 2003. 200(4): p. 448-64.

29. Nowak, G., et al., *Identification of expandable human hepatic progenitors which differentiate into mature hepatic cells in vivo.* Gut, 2005. 54(7): p. 972-9.

30. Pellegrini, G., et al., *p63 identifies keratinocyte stem cells.* Proc Natl Acad Sci U S A, 2001. 98(6): p. 3156-61.

31. Li, A., P.J. Simmons, and P. Kaur, *Identification and isolation of candidate human keratinocyte stem cells based on cell surface phenotype.* Proc Natl Acad Sci U S A, 1998. 95(7): p. 3902-7.

32. Itoh, M., et al., *Generation of keratinocytes from normal and recessive dystrophic epidermolysis bullosa-induced pluripotent stem cells.* Proc Natl Acad Sci U S A, 2011. 108(21): p. 8797-802.

33. Zhou, Q., et al., *Phenformin Promotes Keratinocyte Differentiation* via *the Calcineurin/NFAT Pathway.* J Invest Dermatol, 2021. 141(1): p. 152-163.

34. Walmsley, G.G., et al., *Live fibroblast harvest reveals surface marker shift in vitro.* Tissue Eng Part C Methods, 2015. 21(3): p. 314-21.

35. Mani, S.A., et al., *The epithelial-mesenchymal transition generates cells with properties of stem cells.* Cell, 2008. 133(4): p. 704-15.

36. Samavarchi-Tehrani, P., et al., *Functional genomics reveals a BMP-driven mesenchymal-to-epithelial transition in the initiation of somatic cell reprogramming.* Cell Stem Cell, 2010. 7(1): p. 64-77.

37. Li, R., et al., *A mesenchymal-to-epithelial transition initiates and is required for the nuclear reprogramming of mouse fibroblasts.* Cell Stem Cell, 2010. 7(1): p. 51-63.

38. Saitoh, I., et al., *Induced Tissue-Specific Stem Cells (iTSCs): Their Generation and Possible Use in Regenerative Medicine.* Pharmaceutics, 2021. 13(6).